PET Parametric Imaging: Past, Present, and Future

Guobao Wang,
Department of Radiology, University of California Davis Health, Sacramento, CA 95817, USA

Arman Rahmim,
University of British Columbia, Vancouver, BC, Canada

Roger N. Gunn
Imperial College London and Invicro LLC

Abstract

Positron emission tomography (PET) is actively used in a diverse range of applications in oncology, cardiology, and neurology. The use of PET in the clinical setting focuses on static (single time frame) imaging at a specific time-point post radiotracer injection and is typically considered as semi-quantitative; e.g. standardized uptake value (SUV) measures. In contrast, dynamic PET imaging requires increased acquisition times but has the advantage that it measures the full spatiotemporal distribution of a radiotracer and, in combination with tracer kinetic modeling, enables the generation of multiparametric images that more directly quantify underlying biological parameters of interest, such as blood flow, glucose metabolism, and receptor binding. Parametric images have the potential for improved detection and for more accurate and earlier therapeutic response assessment. Parametric imaging with dynamic PET has witnessed extensive research in the past four decades. In this paper, we provide an overview of past and present activities and discuss emerging opportunities in the field of parametric imaging for the future.

Keywords

PET; parametric imaging; dynamic imaging; kinetic modeling; image reconstruction

I.   Introduction

POSITRON emission tomography (PET) is a molecular imaging modality that enables visualization and measurement of a diverse range of biological processes [1]. A library of existing radiotracers enables quantitative imaging of physiological, biochemical and pharmacological targets and processes including blood flow, metabolism, receptors, transporters, enzymes and labeled drugs themselves. Consequently, PET has wide range of clinical and research applications in oncology [2], cardiology [3] and neurology [4], with glucose metabolic imaging in oncology using ^{18}F-fluorodeoxyglucose (FDG) being the most widespread [5].

gbwang@ucdavis.edu.

Standard application of PET in the clinic yields a three-dimensional (3D) scan that captures the spatial distribution of the radiotracer using static (single-frame) scanning around a certain late time point post-injection [6]. These images are typically quantified using the standardized uptake value (SUV) [7] which normalizes for the injected dose and patient mass or body surface area, and technically can be thought of as parametric imaging with each voxel providing a read-out of the SUV. Static imaging is also prevalent in the realm of clinical trials in neurodegenerative disease with tracers for amyloid and tau being used as entry criteria and pharmacodynamic markers of Phase 2 & 3 trials of novel therapies. Here, SUV data are typically normalized to a reference region devoid of the target protein to generate an SUV ratio (SUVR) image that can also be considered as a parametric image. SUV and SUVR approaches are usually considered as semiquantitative measures as they can be influenced by contaminating factors including patient habitus, scan time, blood flow, etc. and require careful validation before routine deployment [8]. Whilst parametric images such as these are routinely and simply generated from static scans, they are not the focus of this article which concentrates on the generation of parametric images from kinetic analysis of dynamic data.

Dynamic PET imaging measures the four-dimensional (4D: 3D in space and 1D in time) spatiotemporal distribution of a radiotracer in the living body. Parametric imaging from 4D dynamic PET data involves moving beyond SUV images. It can provide a more complete set of biological parameters from the radiotracer using voxel-wise tracer kinetic modeling to accurately quantify the different components of the tracer's passage within the body, e.g. delivery of the tracer into tissue and interaction with protein targets. This process enables generation of multiparametric images that have more direct specificity to the underlying biological parameter of interest than is available from SUV/SUVR composite images.

Parametric imaging has witnessed extensive research in past decades [9]. Despite its great potential, clinical applications of parametric imaging have been hampered due to several limitations [10], such as (1) high noise of dynamic data, (2) need for long acquisitions times, (3) lack of whole-body implementations, and/or (4) limited demonstration of clinical significance beyond SUV.

In recent years, several important technical advances have been made in both algorithms and instrumentation [1]. Examples include advanced dynamic image reconstruction algorithms [9, 11], time-of-flight PET data acquisition [12–14], implementation of whole-body parametric imaging on commercial PET scanners [15], and the recent advent of long axial field-of-view PET scanners (e.g., EXPLORER [16–18], PennPET Explorer [19]) enabling unprecedented sensitivity and simultaneous dynamic imaging of multiple organs [20, 21]. Other kinds of parametric imaging are also possible, such as voxel-wise statistical maps assessing radiotracer uptake (using non-kinetic modeling methods), or voxel-wise images of texture/radiomic features. To date, the field of radiomics [22, 23] has primarily focused on region-of-interest analyses, and voxel-based applications have been less common. We also note that a number of methods and approaches discussed in this review are directly applicable to SPECT imaging, particularly for high-sensitivity dedicated cameras that can collect sufficient projection data in significantly shorter times [24].

Given these advances and the current opportunities, it is appropriate and timely to review past work and promote broader scientific research and clinical applications with parametric imaging. In this article, we provide a brief historic overview of parametric imaging research and discuss emerging research opportunities. The paper is organized as follows. Section II summarizes past and ongoing research activity in the field of PET parametric imaging, including a number of related review articles for various areas of activity as well as available commercial and free software. In Section III, we discuss current challenges and emerging opportunities with new-generation PET scanners. Concluding statements are provided in Section IV.

II. OVERVIEW OF PAST AND ONGOING EFFORTS

A. Overall Research Activity in the Field.

Research on PET parametric imaging started in the 1980's, while kinetic modeling has a longer history. Figure 1(a) depicts a plot of the yearly number of publications relevant to PET parametric imaging from 1980 to 2019. The curves were obtained by using the search terms [(PET) AND (parametric imaging)] in the PubMed database. In addition to original research articles, conference proceeding papers, review papers and book chapters in the database were also included. The activity has increased during this period, following an approximately linear relationship since 1990's.

Figure 1(b) further shows the trends for PET kinetic modeling and parametric imaging as compared to the topic of PET image reconstruction, another critical component of PET imaging. The number of papers on kinetic modeling is generally much higher than that of parametric imaging, which is consistent with the fact that kinetic modeling may be more easily implemented for region of interest analysis while voxel-wise implementation has been more challenging and/or problematic. The ratio of papers between PET image reconstruction and kinetic modeling (and/or parametric imaging) was approximately 1:1 prior to 2005. While work in the area of kinetic modeling has been steadily increasing, image reconstruction has attracted more interests in the past 15 years.

B. Overview of Different Areas of Activity.

We do not intend to provide a comprehensive review of the field of PET parametric imaging in the past 40 years. Rather, we provide brief overviews, in connection with existing review articles, to direct interested readers to more focused topical reviews.

Fig. 2 illustrates the process of parametric imaging which typically consists of raw data acquisition from a scanner, dynamic image reconstruction from projection data, and tracer kinetic modeling. Parametric imaging can be generally classified into two types of methods: indirect and direct. Indirect methods first reconstruct dynamic PET images from the sinogram or list-mode projection data and then perform tracer kinetic modeling pixel by pixel to obtain parametric images. In comparison, direct methods incorporate the kinetic model into the reconstruction formula and estimate parametric images directly from raw projection data.

Parametric imaging methods need to carefully consider (1) selection of appropriate kinetic models, (2) high noise associated with voxel-wise analysis of dynamic imaging data, (3) need for blood input function estimation, (4) lack of whole-body implementation, and (5) increased challenges with patient comfort and motion, due to longer scan times, for parametric imaging. The degree of these challenges varies by application area, e.g. estimation of non-invasive input functions is more straightforward in cardiac applications where large chambers of blood are present in the field of view. Below we discuss a number of trends and approaches related to these challenges.

(1)   Kinetic Modeling Approaches—The underlying principles of tracer kinetic analysis are described in a number of books [25–28] and review articles [10, 29–31].

Compartmental analysis forms the basis for tracer kinetic analysis of PET data and consequently for parametric imaging. Well-established compartmental models in PET include those developed for the quantification of blood flow [32], metabolic rate for glucose [33, 34] and for receptor-ligand binding [35]. These particular models require an arterial blood or plasma input function, with the number of tissue compartments dictated by the physiological, biochemical and physiological properties of the system under study. Other 'reference tissue models' have been developed, particularly for the study of neuroreceptor ligands, with a view to avoiding blood sampling by using a region devoid of target as an alternative input function [36–39]. Both plasma input and reference tissue input models include variants that characterise both reversible and irreversible (i.e. containing a trap that prevents the tracer from being eliminated through the blood) systems. All of these models are described by a system of linear differential equations and lead to solutions that are characterised by the convolution of the input function with a sum of exponentials. These models can be applied to determine parametric images using non-linear optimisers to obtain weighted least squares solutions. However, when it comes to the increased noise present from voxel time activity, more complex models can lead to problems with numerical identifiability and susceptibility to local minima. For this reason, a range of different approaches have been developed that are derived from the same differential equations including graphical methods and basis function methods. Graphical methods, such as Patlak [40, 41], Logan [42], MRTM [43] and MA1 [44] use integral transformations to yield equations whereby the parameter of interest can be derived from a linear regression of an appropriate portion of the dynamic data. Basis function approaches have been applied more generally in the form of spectral analysis [45] and DEPICT [46] along with direct implementation of particular compartmental models such as the 1-tissue compartment and simplified reference tissue model (SRTM) models [38, 39]. The graphical and basis function methods tend to provide improved estimators, but their bias and variance must also be assessed in the presence of noise.

Table I shows a selection of relevant review articles related to PET kinetic modeling and the derivation of a blood input function.

(2)   Noninvasive Estimation of Blood Input Functions—A critical component for kinetic modeling and parametric imaging is the input function. While a blood input function can be obtained with invasive arterial blood sampling (the aim is to avoid this if possible),

research has demonstrated it can be feasible to derive a blood input function from dynamic images without the need of blood sampling or just with one or two blood samples or using population-based input function for certain applications. Zanotti-Fregonara *et al.* [47] specifically summarized the related progress for dynamic brain PET imaging and discussed the remaining challenges. Very recently, Feng *et al.* [48] have summarized the research on using simultaneous optimization strategies for noninvasive estimation of blood input function from dynamic PET image data.

(3)   Improved Image Reconstruction Methods—As compared to a static scan (order of minutes), dynamic PET imaging can successfully employ short scan time frames (e.g., 10–40 seconds per frame) to achieve relatively high temporal resolution for the early phase of a dynamic scan. These short frames are associated with high noise due to limited counting statistics of PET. While the standard reconstruction algorithm for clinical PET scanners is the ordered subset expectation maximization (OSEM) algorithm [49], a wide range of research (Table II) has been devoted to develop more advanced image reconstruction strategies and algorithms in order to suppress noise for parametric imaging. Progresses before 2014 were reviewed in the papers from Tsoumpas et al [50], Rahmim *et al.* [51], Wang and Qi [52], and Reader and Verhaeghe [11]. A more recent review on the same topic is provided by Gallezot *et al.* [9].

Similar to other dynamic imaging such as dynamic contrast-enhanced MRI, frame-based dynamic image reconstruction and post-reconstruction denoising methods are widely researched for dynamic PET [9, 51]. One unique effort specifically in PET is the development of direct parametric image reconstruction algorithms for both linear kinec models (e.g., Patlak plot) and nonlinear kinetic models (e.g., two-tissue compartmental model) [9, 11, 50–52]. Specifically, a nested expectation maximization (Nested EM) [53] algorithm has been adopted for linear parametric image reconstruction on commercial scanners [54].

(4)   Whole-body Dynamic PET—Standard clinical PET scanners commonly have a scanner length of 15–30 cm. Traditionally, whole-body vs. dynamic PET imaging have been thought of as mutually exclusive, with whole-body imaging equating to a static-scan. As a result, while there have been significant efforts in single-bed dynamic PET imaging, the popularity and value of whole-body PET imaging to assess disease distributed throughout the body has implied single-frame (static) imaging. Nonetheless, it is very feasible to perform multi-bed *and* multi-pass imaging with existing PET scanners [55], resulting in the area of dynamic whole-body PET imaging [15]. Rahmim *et al.* recently provided an overview of efforts in this area [15]. Commercial adoption of whole-body Patlak parametric imaging has been implemented on Siemens scanners [54]. This overall approach to imaging is further elaborated in Sec. III.B.

(5)   Motion Correction.—Dynamic PET imaging requires a significantly longer scan time as compared to static imaging. Patient movement, respiratory motion, and cardiac motion may unavoidably exist in dynamic PET imaging and affect the quantitative accuracy of kinetic modeling and parametric imaging. A brief overview of the relevant research on

motion correction for parametric imaging is provided in the review article of Gallezot *et al.* [9].

(6)   Clinical Translation—Many clinical studies have been conducted to investigate potential applications of kinetic modeling and parametric imaging in clinical practice. In particular, dynamic PET with tracer kinetic modeling has been routinely applied in clinical cardiology for assessing myocardial blood flow and myocardial flow reserve [56, 57]. A number of review articles elaborate on the technical perspectives and clinical applications of dynamic cardiac PET [56–60]. A very recent position paper is provided by Murthy *et al.* on clinical quantification of myocardial blood flow using PET [3]. The potential of kinetic quantification in clinical oncology and neurology imaging have also been widely investigated, though not routinely applied in clinical practice yet. The readers are referred to the specific review articles [4, 61]. Section III discusses some relevant emerging opportunities.

C.   Commercial and Open-Source Software

Given significant continued efforts with dynamic imaging, particularly in PET, there exist many software packages that aim to perform kinetic modeling and estimate parameters of interest. The majority of kinetic modeling efforts have been historically in brain and cardiac applications. Nonetheless, applications have been pursued in other single-bed or multi-bed dynamic studies (e.g. see Section III). Table III lists a number of software packages used for a variety of applications and many include the capability for parametric imaging.

We note that in quantitative cardiac imaging (software listed at the bottom of Table III), when performing kinetic modeling of flow quantification, the term 'parametric imaging' is not in common usage. These software provide segmental polar maps, but also commonly depict polar maps at finer scales; this is rarely done per pixel and is averaged over multiple pixels. Therefore, such polar maps are often somewhere between voxelized parametric imaging and segmental flow quantification. Polar maps as such (beyond the usage of mere segmental polar maps) may be useful to see patterns; e.g. sometimes myocardial perfusion defect boundaries may be between segments or territories, and as such, it is useful visually, and physicians may sometimes use it to redefine the vessel boundaries and then obtain averaged regional values over customized regions in the polar map.

D.   New-Generation PET Scanners

In recent years, PET scanner hardware from major vendors has experienced dramatic improvements in effective scanner sensitivity [62–66]. The increase in scanner sensitivity can result in improved image quality for parametric images derived from kinetic modeling. In addition, the axial field of view (AFOV) of PET scanners has increased from a typical 15 cm to 25–30 cm. Table IV lists new commercial scanners from GE [65], Siemens [64], and Canon [66] that have a much longer AFOV than typical prior-generation scanner such as the GE Discovery 690 [67]. These new scanners also have better time-of-flight resolution and can achieve 4–6 times gain in effective sensitivity as compared to a GE 690.

Furthermore, the EXPLORER total-body scanner [17, 18] has a nearly 2-m long AFOV, allowing simultaneous dynamic imaging of the entire body and the PennPET Explorer has an AFOV of 64 cm [19]. These state-of-the-art scanners with improved sensitivity and extended AFOV are providing numerous new opportunities for parametric imaging.

III.   EMERGING OPPORTUNITIES

A.   Organ-specific Parametric Imaging

Dynamic PET and parametric imaging can be well suited to study single organs. Compared to cancer, organ-specific diseases such as Alzheimer's disease and coronary heart disease also affect millions of people worldwide. The brain and heart have a moderate length and can be covered entirely by the AFOV of conventional PET scanners for dynamic imaging. While performance of parametric imaging has been limited by noise, the increased sensitivity of newer scanners, in combination with advanced image reconstruction algorithms, can further improve the data quality of dynamic PET for parametric imaging. In addition, the increased AFOV of new scanners may also improve the extraction of an image-derived input function because larger arteries are included in the AFOV [68].

Other than brain and heart, several other organs are also of tremendous clinical significance for parametric imaging. One such organ is the lung for which the potential of PET kinetic quantification has been investigated (e.g., [69–72]). Respiratory diseases affect a very large population and have a wide spectrum, including chronic obstructive pulmonary disease, acute respiratory distress syndrome, idiopathic pulmonary fibrosis. K_i derived by dynamic FDG-PET kinetic modeling was found to be correlated with pulmonary function and disease severity [72]. Furthermore, accurate correction of lung data for the contribution of blood (~15% of the signal) is critical for quantitative analysis of lung tissue, and kinetic analysis makes this feasible. Another technical aspect of quantitative lung analysis is that the lung commonly has a high fraction of air volume (~70%) and correction for tissue air fraction in addition to blood volume fraction is required. Examples of this can be seen in the work by Coello *et al.* [73] and Holman *et al.* [74]. While conventional PET scanners have a limited scanner length and can only cover a part of the lungs for dynamic imaging, the increased AFOV of new clinical scanners (25–194 cm) makes it now more feasible to perform total-lung dynamic imaging.

Another example of organ-specific parametric imaging is for the liver [75]. Nonalcoholic fatty liver disease (NAFLD) is the most common type of chronic liver disease, affecting an estimated 30% of adults worldwide [76, 77]. 5–10% of patients with NAFLD develop nonalcoholic steatohepatitis (NASH) - a more aggressive form of NAFLD that is associated with an increased risk of end-stage disease (liver failure and liver cancer) and higher liver-related mortality [78, 79]. The hallmark of NASH is liver inflammation (lobular inflammation plus ballooning degeneration) in the setting of hepatic steatosis. Recent studies have demonstrated the potential of using the widely accessible radiotracer ^{18}F-FDG via dynamic PET imaging coupled with tracer kinetic modeling [80, 81]. While SUV or K_i of ^{18}F-FDG did not show promise, the blood-to-tissue transport rate FDG K_1 of the liver demonstrated a strong correlation with histopathological liver inflammation grades [81]. In combination with the ability of CT for evaluating hepatic steatosis, a liver parametric

PET/CT method may have the potential to provide a valuable clinical imaging tool for differentiating NASH from simple fatty liver. One interesting technical aspect of PET liver parametric imaging is that the liver receives dual blood supplies from the hepatic artery and the portal vein [75], which should be taken into account in tracer kinetic modeling [75, 80].

B. Whole-Body and Total-Body Parametric Imaging

Dynamic whole-body (DWB) PET imaging, involving multi-bed multi-pass imaging, enables whole-body parametric imaging using existing scanners (Sec. II.B.4). The scan can begin at or after radiotracer injection. When beginning at injection, one can typically first perform single-bed dynamic PET imaging over the heart (e.g. for ~5 minutes) followed by multiple rapid whole-body PET passes. This enables use of the heart's blood pool (left ventricle or atrium) to non-invasively quantify the blood input function (BIF) at early times, with DWB PET naturally imaging the heart at later times to capture the tail of the curve as well. Alternatively, other blood pools can be considered; e.g. carotid arteries, ascending aorta, thoracic (descending) aorta, or abdominal aorta as blood pools [82, 83]. This enables placement of initial single-bed scanning over the pathology of interest for more elaborate assessment (beyond Patlak models) [84].

On the other hand, one may perform DWB PET scan using delayed imaging (i.e. not starting at injection) and utilize population-based BIFs for early times. It is worth noting that: (i) population-based BIFs can be personalized in DWB PET, as they can be scaled based on the later multi-time-point scans over the heart (or other blood pools) in each individual subject; (ii) in Patlak (as well as generalized Patlak [85]) parametric imaging, only the area-under the BIF at early times post-injection needs to be estimated (not accurate individual BIF values at early times), and error propagation has been shown to be limited [86]. Overall, DWB PET parametric imaging is applicable to both PET/CT and PET/MRI, in both step-and-shoot and continuous-bed-motion PET scanning modes (e.g. see Table I in [15]), and can be used to generate conventional SUV images simultaneously by summation of the dynamic frames [87].

An interesting new frontier, with significant excitement, is total-body PET imaging [17, 18]. A PET scanner with a very large AFOV enables significantly enhanced sensitivity (e.g. by up to a factor of ~40 for 2-meters AFOV), opening up new possibilities to reduce administered doses, shorten scan times and/or enhance image quality [20, 88, 89]. Another implication is that single-bed dynamic PET scanning of the entire body becomes possible [21]. The significantly improved sensitivity, in turn, enables generation of higher-quality parametric images. Furthermore, models beyond Patlak analysis can be used, to estimate different microparameters [90]. Figure 3 shows an example of parametric imaging of both macro kinetic parameter K_i (FDG net influx rate) and micro kinetic parameters K_1 (blood-to-tissue transport rate) and V_b (fractional blood volume) from a dynamic ^{18}F-FDG dynamic PET scan on the EXPLORER scanner [90].

There is an interesting potential opportunity with total-body dynamic imaging to address the challenge of estimating a true parent plasma input function for radiotracers with metabolites. To explain the challenge, we note that it is relatively straightforward to assay whole blood activity from vascular regions for tracers such as ^{18}F-FDG where the plasma and whole

blood are in equilibrium and no blood-based metabolites exist. However, for other radiotracers this is more complicated. In particular when metabolism of the radiotracer leads to the presence of radiolabeled metabolites in the blood, then corrections are necessary so that a plasma parent input function can be derived for kinetic modeling. To date, this has been performed by separate high-performance liquid chromatography (HPLC) analyses of discrete blood samples, but this defeats the purpose of enabling truly non-invasive quantification. We note that with fully whole-body dynamic imaging systems such as the EXPLORER, there is a potential opportunity to develop whole-body multi-organ kinetic models that are able to accurately model the metabolism of the radiotracer in the periphery enabling accurate estimation of the required parent plasma input function.

Overall, it remains to be seen whether whole/total-body parametric PET imaging will be deployed routinely in the clinic. This is because as newer generation PET scanners enable ever-higher-quality parametric PET images, they continue at the same time to push down the time needed for standard SUV PET imaging. It has thus been argued that applications need to demonstrate significantly increased value for more widespread usage of parametric PET imaging (see point-counterpoint discussion [91]). Whole/total-body parametric PET imaging certainly has significant potential and may also enable discoveries and insights into systemic disease as well systemic interactions and responses; e.g. gut-brain [92] or heart-brain [93] axes.

C. Multi-tracer Parametric Imaging

While the majority of PET studies use a single radiotracer, PET imaging with two (or more) different radiotracers have also found interesting and useful applications in the clinic (e.g., [94, 95]). Different tracers may complement each other to provide a more comprehensive characterization of a disease. For example, myocardial viability assessment requires a perfusion-specific radiotracer (e.g., ^{82}Rb-chloride) scan and a metabolic scan with ^{18}F-FDG to evaluate perfusion-metabolism mismatch for determining myocardial hibernation in the clinic [96].

The typical way of doing a dual-tracer (or multi-tracer) study is to acquire the scans for each tracer in separate imaging sessions or even on separate days (e.g., [97, 98]). This is because the residual activity of the first tracer remains for the subsequent tracer scans if the separation time between two scans is not long enough. This method, however, is resource intensive and burdensome for the patient.

Single-scan dual-tracer (and multi-tracer) methods with staggered injection have attracted interests in the last two decades [95, 99, 100]. Instead of being totally separated, the injection of two tracers are offset with a much-shortened separation time (e.g., several minutes to 30 minutes) so that a single scanning session becomes feasible. In order to recover separate images of each tracer from the same scan, dynamic imaging and kinetic modeling can be used to identify and separate the two tracer signals from each other [100–109]. Such a methodology has been applied to dual-tracer or multi-tracer brain imaging [100, 101, 110–112] and tumor imaging [99, 113–116]. A similar method has also been explored for multiple injections of a flow tracer, e.g., for rest-stress myocardial perfusion imaging [117, 118]. It is also possible to utilize such parametric imaging, merely as an

intermediate step, to generate two standard relative-perfusion rest and stress images from a single PET scan (e.g., by commercial clinical software mfiVerse™).

While the robustness of dual-tracer methods has been limited by data noise, the dramatically increased sensitivity of new PET scanners is offering new opportunities to make this framework more robust and feasible for clinical use.

D. Single-tracer Multiparametric Imaging

Conventionally parametric imaging of tracer kinetics has mainly focused on equilibrium parameters, e.g. the net irreversible uptake rate constant, K_i, for ^{18}F-FDG to quantify glucose metabolism. The K_i is frequently estimated from the Patlak graphical plot, which also allows for the estimation of an intercept value that is complicated by the fact that it is actually a mix of blood volume and the steady state distribution volume. The potential of parametric imaging for multiparametric characterization can be further explored through the deployment of full compartmental modeling in which microparameters are also estimated. These models are more accurately able to directly estimate the underlying biological processes such as the delivery K_1, which denotes the rate of radiotracer transport from plasma to tissue, and the steady state distribution volume, V_{SS}, which may increase the information available for different applications.

Early studies have demonstrated that K_1 could approximate blood flow in tumors for ^{18}F-FDG [119–123]. Correlation of FDG K_1 with blood flow was also reported in the brain [124] and liver [125]. A recent study also attempted to develop cardiac FDG K_1 as a surrogate of myocardial blood flow, and combine it with glucose metabolic imaging, to enable simultaneous imaging of myocardial perfusion-metabolism using only ^{18}F-FDG [126]. Such a single-tracer multiparametric imaging method has the potential to reduce imaging time, cost and radiation exposure as compared to a two-tracer protocol [96] or dual modalities [127].

Parametric imaging of K_1 or relative delivery rate R_1 of beta amyloid tracers (e.g., ^{18}F-florbetapir [128–130], ^{11}C-PiB [131–133], ^{18}F-florbetpen [134]) or tau tracers (e.g., ^{18}F-flortaucipir [135], ^{18}F-PI-2620 [136]) is also being studied as a surrogate of cerebral blood flow to provide a single-tracer dual-phase imaging methodology in brain imaging of neurodegenerative diseases. This holds the promise of providing complementary information on both blood flow and misfolded protein changes in neurodegenerative disease using a single tracer that has only been achieved previously through the application of multiple tracers [130, 137, 138]. The same single-tracer multiparametric imaging principle is also applicable to many other radiotracers not mentioned above, such as ^{18}F-MISO [139].

E. High-Temporal Resolution Kinetic Modeling and Parametric Imaging

Standard dynamic PET imaging often uses a moderate temporal resolution of 10–40 seconds (or poorer) per time frame (see [123, 140] for example). This is aimed at reaching a balance between image noise and the necessary temporal resolution for kinetic modeling. High-temporal resolution (HTR; 1–2 seconds/frame or better) dynamic imaging has rarely been explored in clinical dynamic PET studies because of the concern over low signal-to-noise ratio and lack of clinical applications.

Renewed interests are growing in the PET field to develop HTR dynamic imaging by using improved dynamic image reconstruction algorithms [141], overlapping temporal framing strategies [142, 143] or the boosted sensitivity from new PET scanners [18]. Example dynamic images extracted from an HTR dynamic FDG-PET scan on the EXPLORER scanner can be found in [18] and [21]. Figure 4 shows an example of HTR time activity curves of different organs from an EXPLORER total-body dynamic scan. Combining the ultra-high sensitivity of the EXPLORER [17, 18] with the kernel method for dynamic image reconstruction [144], recent work by Zhang *et al.* [145] has even demonstrated the feasibility of total-body sub-second (0.1s per frame) dynamic PET imaging.

With HTR dynamic imaging, more physiological processes may be captured, hence requiring potentially new kinetic modeling [146–148]. HTR imaging combined with kinetic modeling will potentially further enable quantification of tissue delivery processes and more accurately estimate and correct for blood-based signals. Recent studies [146, 147] have demonstrated that HTR dynamic imaging could enable the application of time-varying kinetic models to analyze early-dynamic FDG-PET data for the derivation of information on both blood flow and the glucose transport rate. Thus, it may become possible to derive three different physiological parameters from a dynamic ^{18}F-FDG scan – blood flow, glucose transport, and glucose metabolism – using HTR dynamic PET imaging. Whilst these new opportunities have been discussed in the context of ^{18}F-FDG, they will provide similar opportunities for a wide range of radiotracers.

Note that with increased temporal resolution, pixel-level noise in the spatial domain may become higher. Thus, it is necessary to continue to develop new dynamic image reconstruction algorithms. Among various directions, deep learning-based methods have been embraced and received enthusiasms in the field. Interested readers are referred to two recent review articles [149, 150] for details.

IV. CONCLUSION

PET parametric imaging, in its ~40-year history, has witnessed substantial progress with noise suppression, whole-body implementation, noninvasive derivation of input functions, and reconstruction-based methods, including implementations on vendor scanners. With recent advances in high-sensitivity scanners and extended axial field of view, including the advent of total-body PET, many exciting opportunities are emerging for the application of parametric imaging in research and clinical arenas.

REFERENCES

[1]. Jones T and Townsend D, "History and future technical innovation in positron emission tomography," Journal of Medical Imaging, vol. 4, no. 1, 1 2017, Art no. 011013, doi: 10.1117/1.jmi.4.1.011013.

[2]. Gambhir SS, "Molecular imaging of cancer with positron emission tomography," Nature Reviews Cancer, vol. 2, no. 9, pp. 683–693, 9 2002, doi: 10.1038/nrc882. [PubMed: 12209157]

[3]. Daou D et al., "Clinical Quantification of Myocardial Blood Flow Using PET: Joint Position Paper of the SNMMI Cardiovascular Council and the ASNC," Journal of Nuclear Cardiology, vol. 25, no. 1, pp. 269–297, 2 2018, doi: 10.1007/s12350-017-1110-x. [PubMed: 29243073]

[4]. Gunn RN, Slifstein M, Searle GE, and Price JC, "Quantitative imaging of protein targets in the human brain with PET," Phys. Med. Biol, vol. 60, no. 22, pp. R363–R411, 11 2015, doi: 10.1088/0031-9155/60/22/r363. [PubMed: 26513176]

[5]. Gambhir SS, Czernin J, Schwimmer J, Silverman DHS, Coleman RE, and Phelps ME, "A tabulated summary of the FDG PET literature," J. Nucl. Med, vol. 42, no. 5, pp. 1S–93S, 5 2001. [Online]. Available: <Go to ISI>://WOS:000168669400001. [PubMed: 11483694]

[6]. Fletcher JW et al., "Recommendations on the use of F-18-FDG PET in oncology," J. Nucl. Med, vol. 49, no. 3, pp. 480–508, 3 2008, doi: 10.2967/jnumed.107.047787. [PubMed: 18287273]

[7]. Huang S-C, "Anatomy of SUV," Nucl Med Biol, vol. 27, no. 7, pp. 643–646, 2000. [Online]. Available: http://linkinghub.elsevier.com/retrieve/pii/S0969805100001554?showall=true. [PubMed: 11091106]

[8]. Keyes JW Jr., "SUV: Standard Uptake or Silly Useless Value?," J Nucl Med, vol. 36, no. 10, pp. 1836–1839, 10 1, 1995 1995. [Online]. Available: http://jnm.snmjournals.org. [PubMed: 7562051]

[9]. Gallezot JD, Lu YH, Naganawa M, and Carson RE, "Parametric Imaging With PET and SPECT," IEEE Transactions on Radiation and Plasma Medical Sciences, vol. 4, no. 1, pp. 1–23, 2020.

[10]. Kotasidis FA, Tsoumpas C, and Rahmim A, "Advanced kinetic modelling strategies: towards adoption in clinical PET imaging," Clinical and Translational Imaging, vol. 2, no. 3, pp. 219–237, 6 2014, doi: 10.1007/s40336-014-0069-8.

[11]. Reader AJ and Verhaeghe J, "4D image reconstruction for emission tomography," Phys. Med. Biol, vol. 59, no. 22, pp. R371–R418, 11 21 2014, doi: 10.1088/0031-9155/59/22/r371. [PubMed: 25361380]

[12]. Surti S, "Update on Time-of-Flight PET Imaging," J. Nucl. Med, vol. 56, no. 1, pp. 98–105, 1 2015, doi: 10.2967/jnumed.114.145029. [PubMed: 25525181]

[13]. Vandenberghe S, Mikhaylova E, D'Hoe E, Mollet P, and Karp JS, "Recent developments in time-of-flight PET," Ejnmmi Physics, vol. 3, no. 1, 2 2016, Art no. 3, doi: 10.1186/s40658-016-0138-3.

[14]. Lecoq P, "Pushing the Limits in Time-of-Flight PET Imaging," IEEE Transactions on Radiation and Plasma Medical Sciences, vol. 1, no. 6, pp. 473–485, 11 2017, doi: 10.1109/trpms.2017.2756674.

[15]. Rahmim A et al., "Dynamic whole-body PET imaging: principles, potentials and applications," Eur J Nucl Med Mol I, vol. 46, no. 2, pp. 501–518, 2019.

[16]. Cherry S, Badawi R, Karp J, Moses W, Price P, and Jones T, "Total-body imaging: Transforming the role of PET in translational medicine," Science Translational Medicine, vol. 9, no. 381, p. eaaf6169, 2017. [PubMed: 28298419]

[17]. Cherry SR, Jones T, Karp JS, Qi J, Moses WW, and Badawi RD, "Total-body PET: Maximizing sensitivity to create new opportunities for clinical research and patient care," J Nucl Med, vol. 59, no. 1, pp. 3–12, 2018. [PubMed: 28935835]

[18]. Badawi RD et al., "First human imaging studies with the EXPLORER total-body PET scanner," J Nucl Med, vol. 60, no. 3, pp. 299–303, 2019. [PubMed: 30733314]

[19]. Pantel AR et al., "PennPET Explorer: Human Imaging on a Whole-Body Imager," J. Nucl. Med, vol. 61, no. 1, pp. 144–151, 1 2020, doi: 10.2967/jnumed.119.231845. [PubMed: 31562224]

[20]. Surti S, Pantel AR, and Karp JS, "Total Body PET: Why, How, What for?," IEEE Transactions on Radiation and Plasma Medical Sciences, vol. 4, no. 3, pp. 283–292, 5 2020, doi: 10.1109/trpms.2020.2985403. [PubMed: 33134653]

[21]. Zhang X et al., "Total-body dynamic reconstruction and parametric imaging on the uEXPLORER," J Nucl Med, vol. 61, no. 2, pp. 285–291, 2020. [PubMed: 31302637]

[22]. Hatt M, Tixier F, Pierce L, Kinahan PE, Le Rest CC, and Visvikis D, "Characterization of PET/CT images using texture analysis: the past, the presenta... any future?," (in English), Eur J Nucl Med Mol I, vol. 44, no. 1, pp. 151–165, 1 2017, doi: 10.1007/s00259-016-3427-0.

[23]. Parekh V and Jacobs MA, "Radiomics: a new application from established techniques," Expert review of precision medicine and drug development, vol. 1, no. 2, pp. 207–226, 2016. [PubMed: 28042608]

[24]. Wells RG et al., "Dynamic SPECT measurement of absolute myocardial blood flow in a porcine model," J Nucl Med, vol. 55, no. 10, pp. 1685–1691, 2014. [PubMed: 25189340]

[25]. Lassen N and Perl W, Tracer kinetic methods in medical physiology. New York: Raven Press, 1979.

[26]. Huang S and Phelps M, "Principles of tracer kinetic modeling in positron emission tomography and autoradiography," in Positron Emission Tomography and Autoradiography: Principles and Applications for the Brain and Heart, Phelps ME, Mazziotta J, and Schelbert H Eds. New York: Raven Press, 1986, pp. 287–346.

[27]. Morris ED, Endres CJ, Schmidt KC, Christian BT, Muzic RF, and Fisher RE, "Kinetic modeling in positron emission tomography," in Emission Tomography: The Fundamentals of PET and SPECT, Wermick MN and A. JN Eds.: Elsevier Inc., 2004, pp. 499–540.

[28]. Carson RE, "Tracer Kinetic Modeling in PET," in Positron Emission Tomography, Bailey DL, Townsend DW, Valk PE, and Maisey MN Eds. London: Springer, 2005.

[29]. Gunn RN, Gunn SR, and Cunningham VJ, "Positron emission tomography compartmental models," J. Cereb. Blood Flow Metab, vol. 21, no. 6, pp. 635–652, 6 2001, doi: 10.1097/00004647-200106000-00002. [PubMed: 11488533]

[30]. Ichise M, Meyer JH, and Yonekura Y, "An introduction to PET and SPECT neuroreceptor quantification models," J. Nucl. Med, vol. 42, no. 5, pp. 755–763, 5 2001. [Online]. Available: <Go to ISI>://WOS:000168594800021. [PubMed: 11337572]

[31]. Burger C and Buck A, "Requirements and implementation of a flexible kinetic modeling tool," J. Nucl. Med, vol. 38, no. 11, pp. 1818–1823, 11 1997. [Online]. Available: <Go to ISI>://WOS:A1997YF97100043. [PubMed: 9374364]

[32]. Kety SS and Schmidt CF, "THE NITROUS OXIDE METHOD FOR THE QUANTITATIVE DETERMINATION OF CEREBRAL BLOOD FLOW IN MAN - THEORY, PROCEDURE AND NORMAL VALUES," Journal of Clinical Investigation, vol. 27, no. 4, pp. 476–483, 1948, doi: 10.1172/jci101994.

[33]. Sokoloff L et al., "DEOXYGLUCOSE-C-14 METHOD FOR MEASUREMENT OF LOCAL CEREBRAL GLUCOSE-UTILIZATION - THEORY, PROCEDURE, AND NORMAL VALUES IN CONSCIOUS AND ANESTHETIZED ALBINO-RAT," Journal of Neurochemistry, vol. 28, no. 5, pp. 897–916, 1977, doi: 10.1111/j.1471-4159.1977.tb10649.x. [PubMed: 864466]

[34]. Phelps ME, Huang SC, Hoffman EJ, Selin C, Sokoloff L, and Kuhl DE, "TOMOGRAPHIC MEASUREMENT OF LOCAL CEREBRAL GLUCOSE METABOLIC-RATE IN HUMANS WITH (F-18)2-FLUORO-2-DEOXY-D-GLUCOSE - VALIDATION OF METHOD," Ann. Neurol, vol. 6, no. 5, pp. 371–388, 1979, doi: 10.1002/ana.410060502. [PubMed: 117743]

[35]. Mintun MA, Raichle ME, Kilbourn MR, Wooten GF, and Welch MJ, "A QUANTITATIVE MODEL FOR THE INVIVO ASSESSMENT OF DRUG-BINDING SITES WITH POSITRON EMISSION TOMOGRAPHY," Ann. Neurol, vol. 15, no. 3, pp. 217–227, 1984, doi: 10.1002/ana.410150302. [PubMed: 6609679]

[36]. Blomqvist G, Pauli S, Farde L, Ericksson L, Persson A, and Halldin C, "Dynamic models of reversible ligand binding," in Clinical Research and Clinical Diagnosis, Beckers C, Goffinet A, and Bol A Eds.: Kluwer Academic Publishers, 1989.

[37]. Cunningham VJ, Hume SP, Price GR, Ahier RG, Cremer JE, and Jones AKP, "COMPARTMENTAL ANALYSIS OF DIPRENORPHINE BINDING TO OPIATE RECEPTORS IN THE RAT INVIVO AND ITS COMPARISON WITH EQUILIBRIUM DATA INVITRO," J. Cereb. Blood Flow Metab, vol. 11, no. 1, pp. 1–9, 1 1991, doi: 10.1038/jcbfm.1991.1. [PubMed: 1845764]

[38]. Lammertsma AA and Hume SP, "Simplified reference tissue model for PET receptor studies," Neuroimage, vol. 4, no. 3, pp. 153–158, 12 1996, doi: 10.1006/nimg.1996.0066. [PubMed: 9345505]

[39]. Gunn RN, Lammertsma AA, Hume SP, and Cunningham VJ, "Parametric imaging of ligand-receptor binding in PET using a simplified reference region model," Neuroimage, vol. 6, no. 4, pp. 279–287, 11 1997, doi: 10.1006/nimg.1997.0303. [PubMed: 9417971]

[40]. Patlak CS, Blasberg RG, and Fenstermacher JD, "Graphical evaluation of blood-to-brain transfer constants from multiple-time uptake data," J. Cereb. Blood Flow Metab, vol. 3, no. 1, pp. 1–7, 1983 1983. [Online]. Available: <Go to ISI>://WOS:A1983QD19900001. [PubMed: 6822610]

[41]. Patlak CS and Blasberg RG, "Graphical Evaluation of Blood-to-Brain Transfer Constants from Multiple-Time Uptake Data. Generalizations," J. Cereb. Blood Flow Metab, vol. 5, no. 4, pp. 584–590, 1985, doi: 10.1038/jcbfm.1985.87. [PubMed: 4055928]

[42]. Logan J, Fowler JS, Volkow ND, Ding YS, Wang GJ, and Alexoff DL, "A strategy for removing the bias in the graphical analysis method," J. Cereb. Blood Flow Metab, vol. 21, no. 3, pp. 307–320, 3 2001. [Online]. Available: <Go to ISI>://WOS:000167347900014. [PubMed: 11295885]

[43]. Ichise M et al., "Linearized reference tissue parametric Imaging methods: Application to C-11 DASB positron emission tomography studies of the serotonin transporter in human brain," J. Cereb. Blood Flow Metab, vol. 23, no. 9, pp. 1096–1112, 9 2003, doi: 10.1097/01.wcb.0000085441.37552.ca. [PubMed: 12973026]

[44]. Ichise M, Toyama H, Innis RB, and Carson RE, "Strategies to improve neuroreceptor parameter estimation by linear regression analysis," J. Cereb. Blood Flow Metab, vol. 22, no. 10, pp. 1271–1281, 10 2002. [Online]. Available: <Go to ISI>://WOS:000178399200015. [PubMed: 12368666]

[45]. Cunningham VJ and Jones T, "SPECTRAL-ANALYSIS OF DYNAMIC PET STUDIES," J. Cereb. Blood Flow Metab, vol. 13, no. 1, pp. 15–23, 1 1993, doi: 10.1038/jcbfm.1993.5. [PubMed: 8417003]

[46]. Gunn RN, Gunn SR, Turkheimer FE, Aston JAD, and Cunningham TJ, "Positron emission tomography compartmental models: A basis pursuit strategy for kinetic modeling," J. Cereb. Blood Flow Metab, vol. 22, no. 12, pp. 1425–1439, 12 2002, doi: 10.1097/01.wcb.0000045042.03034.42. [PubMed: 12468888]

[47]. Zanotti-Fregonara P, Chen K, Liow JS, Fujita M, and Innis RB, "Image-derived input function for brain PET studies: many challenges and few opportunities," J. Cereb. Blood Flow Metab, vol. 31, no. 10, pp. 1986–1998, 10 2011, doi: 10.1038/jcbfm.2011.107. [PubMed: 21811289]

[48]. Feng D, Chen K, and Wen L, "Non-invasive Input Function Acquisition and Simultaneous Estimations with Physiological Parameters for PET Quantification: A Brief Review," IEEE Transactions on Radiation and Plasma Medical Sciences, vol. Early access, pp. 1–1, 21 7 2020, doi: 10.1109/TRPMS.2020.3010844.

[49]. Hudson HM and Larkin RS, "ACCELERATED IMAGE-RECONSTRUCTION USING ORDERED SUBSETS OF PROJECTION DATA," IEEE Trans. Med. Imaging, vol. 13, no. 4, pp. 601–609, 12 1994, doi: 10.1109/42.363108. [PubMed: 18218538]

[50]. Tsoumpas C, Turkheimer FE, and Thielemans K, "A survey of approaches for direct parametric image reconstruction in emission tomography," Medical Physics, vol. 35, no. 9, pp. 3963–3971, 9 2008, doi: 10.1118/1.2966349. [PubMed: 18841847]

[51]. Rahmim A, Tang J, and Zaidi H, "Four-dimensional (4D) image reconstruction strategies in dynamic PET: Beyond conventional independent frame reconstruction," Medical Physics, vol. 36, no. 8, pp. 3654–3670, 8 2009, doi: 10.1118/1.3160108. [PubMed: 19746799]

[52]. Wang G and Qi J, "Direct estimation of kinetic parametric images for dynamic PET.," Theranostics, vol. 3, no. 10, pp. 802–15, 2013–11–20 2013, doi: 10.7150/thno.5130. [PubMed: 24396500]

[53]. Wang G and Qi J, "Acceleration of the direct reconstruction of linear parametric images using nested algorithms," Phys. Med. Biol, vol. 55, no. 5, pp. 1505–1517, 3 7 2010, doi: 10.1088/0031-9155/55/5/016. [PubMed: 20157226]

[54]. Hu J, Panin V, Smith A, and e. al., "Design and Implementation of Automated Clinical Whole Body Parametric PET with Continuous Bed Motion," IEEE Transactions on Radiation and Plasma Medical Sciences, vol. Early access, pp. 1–1, 14 5 2020 2020, doi: 0.1109/TRPMS.2020.2994316.

[55]. Karakatsanis NA, Lodge MA, Tahari AK, Zhou Y, Wahl RL, and Rahmim A, "Dynamic whole body PET parametric imaging: I. Concept, acquisition protocol optimization and clinical application," Phys. Med. Bio, vol. 58, no. 20, pp. 7391–7418 2013. [PubMed: 24080962]

[56]. Di Carli MF, Dorbala S, Meserve J, El Fakhri G, Sitek A, and Moore SC, "Clinical myocardial perfusion PET/CT," J. Nucl. Med, vol. 48, no. 5, pp. 783–793, 5 2007, doi: 10.2967/jnumed.106.032789. [PubMed: 17475968]

[57]. Gullberg GT, Shrestha UM, and Seo Y, "Dynamic cardiac PET imaging: Technological improvements advancing future cardiac health," Journal of Nuclear Cardiology, vol. 26, no. 4, pp. 1292–1297, 8 2019, doi: 10.1007/s12350-018-1201-3. [PubMed: 29388118]

[58]. Slomka P et al., "Comparison of clinical tools for measurements of regional stress and rest myocardial blood flow assessed with 13N-ammonia PET/CT.," J. Nucl. Med, vol. 53, no. 2, pp. 171–81, 2012. [PubMed: 22228795]

[59]. Schindler TH, Quercioli A, Valenta I, Ambrosio G, Wahl RL, and Dilsizian V, "Quantitative Assessment of Myocardial Blood Flow-Clinical and Research Applications," Seminars in Nuclear Medicine, vol. 44, no. 4, pp. 274–293, 7 2014, doi: 10.1053/j.semnuclmed.2014.04.002. [PubMed: 24948151]

[60]. Murthy VL et al., "Comparison and Prognostic Validation of Multiple Methods of Quantification of Myocardial Blood Flow with Rb-82 PET," J. Nucl. Med, vol. 55, no. 12, pp. 1952–1958, 12 2014, doi: 10.2967/jnumed.114.145342. [PubMed: 25429160]

[61]. Dimitrakopoulou-Strauss A, Pan LY, and Sachpekidis C, "Kinetic modeling and parametric imaging with dynamic PET for oncological applications: general considerations, current clinical applications, and future perspectives," European Journal of Nuclear Medicine and Molecular Imaging, doi: 10.1007/s00259-020-04843-6.

[62]. Rausch I, Ruiz A, Valverde-Pascual I, Cal-Gonzalez J, Beyer T, and Carrio I, "Performance Evaluation of the Vereos PET/CT System According to the NEMA NU2–2012 Standard," J. Nucl. Med, vol. 60, no. 4, pp. 561–567, 4 2019, doi: 10.2967/jnumed.118.215541. [PubMed: 30361382]

[63]. Chen SG, Hu PC, Gu YS, Yu HJ, and Shi HC, "Performance characteristics of the digital uMI550 PET/CT system according to the NEMA NU2–2018 standard," Ejnmmi Physics, vol. 7, no. 1, 6 2020, Art no. 43, doi: 10.1186/s40658-020-00315-w.

[64]. van Sluis J et al., "Performance characteristics of the digital Biograph Vision PET/CT system," J. Nucl. Med, vol. 60, no. 7, pp. 1031–1036, 2019. [PubMed: 30630944]

[65]. Pan T et al., "Performance evaluation of the 5-Ring GE Discovery MI PET/CT system using the national electrical manufacturers association NU 2–2012 Standard," Medical Physics, vol. 46, no. 7, pp. 3025–3033, 2019. [PubMed: 31069816]

[66]. Bai B, Iatrou M, Kolthammer J, and Winkler M, "Initial Clinical Experience with the Canon Cartesion Prime Digital PET/CT," Journal Nuclear Medicine, vol. 61, no. supplement 1, p. 1505, 2020.

[67]. Bettinardi V, Presotto L, Rapisarda E, Picchio M, Gianolli L, and Gilardi MC, "Physical Performance of the new hybrid PET/CT Discovery-690," Medical Physics, vol. 38, no. 10, pp. 5394–5411, 10 2011, doi: 10.1118/1.3635220. [PubMed: 21992359]

[68]. Li E et al., "Identification and comparison of image-derived input functions using total-body PET," Journal Nuclear Medicine, vol. 60, no. supplement 1, p. 520, 2019.

[69]. de Prost N, Tucci MR, and Melo MFV, "Assessment of Lung Inflammation With F-18-FDG PET During Acute Lung Injury," American Journal of Roentgenology, vol. 195, no. 2, pp. 292–300, 8 2010, doi: 10.2214/ajr.10.4499. [PubMed: 20651183]

[70]. de Prost N et al., "F-18-FDG Kinetics Parameters Depend on the Mechanism of Injury in Early Experimental Acute Respiratory Distress Syndrome," J. Nucl. Med, vol. 55, no. 11, pp. 1871–1877, 11 2014, doi: 10.2967/jnumed.114.140962. [PubMed: 25286924]

[71]. Braune A et al., "Comparison of Static and Dynamic F-18-FDG PET/CT for Quantification of Pulmonary Inflammation in Acute Lung Injury," J. Nucl. Med, vol. 60, no. 11, pp. 1629–1634, 11 2019, doi: 10.2967/jnumed.119.226597. [PubMed: 31053684]

[72]. Chen DL et al., "Quantification of Lung PET Images: Challenges and Opportunities," J. Nucl. Med, vol. 58, no. 2, pp. 201–207, 2 2017, doi: 10.2967/jnumed.116.184796. [PubMed: 28082432]

[73]. Coello C et al., "Quantitative analysis of dynamic F-18-FDG PET/CT for measurement of lung inflammation," Ejnmmi Research, vol. 7, 5 2017, Art no. 47, doi: 10.1186/s13550-017-0291-2.

[74]. Holman BF et al., "Improved correction for the tissue fraction effect in lung PET/CT imaging," Phys. Med. Biol, vol. 60, no. 18, pp. 7387–7402, 9 2015, doi: 10.1088/0031-9155/60/18/7387. [PubMed: 26350580]

[75]. Keiding S, "Bringing Physiology into PET of the Liver," J. Nucl. Med, vol. 53, no. 3, pp. 425–433, 3 2012, doi: 10.2967/jnumed.111.100214. [PubMed: 22323781]

[76]. Chalasani N et al., "The diagnosis and management of nonalcoholic fatty liver disease: Practice guidance from the American Association for the Study of Liver Diseases," Hepatology, vol. 67, no. 1, pp. 328–357, 1 2018, doi: 10.1002/hep.29367. [PubMed: 28714183]

[77]. Rinella ME, "Nonalcoholic Fatty Liver Disease A Systematic Review," JAMA-Journal of the American Medical Association, vol. 313, no. 22, pp. 2263–2273, 6 2015, doi: 10.1001/jama.2015.5370.

[78]. Michelotti GA, Machado MV, and Diehl AM, "NAFLD, NASH and liver cancer," Nature Reviews Gastroenterology & Hepatology, vol. 10, no. 11, pp. 656–665, 11 2013, doi: 10.1038/nrgastro.2013.183. [PubMed: 24080776]

[79]. Wree A, Broderick L, Canbay A, Hoffman HM, and Feldstein AE, "From NAFLD to NASH to cirrhosis - new insights into disease mechanisms," Nature Reviews Gastroenterology & Hepatology, vol. 10, no. 11, pp. 627–636, 11 2013, doi: 10.1038/nrgastro.2013.149. [PubMed: 23958599]

[80]. Wang GB, Corwin MT, Olson KA, Badawi RD, and Sarkar S, "Dynamic PET of human liver inflammation: impact of kinetic modeling with optimization-derived dual-blood input function," Phys. Med. Biol, vol. 63, no. 15, p. 155004, 2018, doi: 10.1088/1361-6560/aac8cb. [PubMed: 29847315]

[81]. Sarkar S, Corwin MT, Olson KA, Badawi RD, and Wang GB, "Pilot study to diagnose non-alcoholic steatohepatitis with dynamic 18F-fluorodeoxyglucose positron emission tomography," American Journal of Roentgenology, vol. 212, no. 3, pp. 529–537, 2019. [PubMed: 30673340]

[82]. Zanotti-Fregonara P et al., "Comparison of eight methods for the estimation of the image-derived input function in dynamic [18F]-FDG PET human brain studies," Journal of Cerebral Blood Flow & Metabolism, vol. 29, no. 11, pp. 1825–1835, 2009. [PubMed: 19584890]

[83]. de Geus-Oei L-F et al., "Comparison of image-derived and arterial input functions for estimating the rate of glucose metabolism in therapy-monitoring 18F-FDG PET studies," J Nucl Med, vol. 47, no. 6, pp. 945–949, 2006. [PubMed: 16741303]

[84]. Zaker N, Kotasidis F, Garibotto V, and Zaidi H, "Assessment of Lesion Detectability in Dynamic Whole-Body PET Imaging Using Compartmental and Patlak Parametric Mapping," Clinical Nuclear Medicine, vol. 45, no. 5, pp. e221–e231, 2020. [PubMed: 32108696]

[85]. Karakatsanis NA, Casey ME, Lodge MA, Rahmim A, and Zaidi H, "Whole-body direct 4D parametric PET imaging employing nested generalized Patlak expectation–maximization reconstruction," Phys Med Biol, vol. 61, no. 15, p. 5456, 2016. [PubMed: 27383991]

[86]. Yao S et al., "Simplified Protocol for Whole Body Patlak Parametric Imaging with 18F-FDG PET/CT: Feasibility and Error Analysis," Med Phys, 2020.

[87]. Karakatsanis NA, Casey ME, Knesaurek K, Fayad ZA, and Kostakoglu L, "SUV/Patlak-4D whole-body PET/CT dynamic and parametric imaging: clinical demonstration and validation of SUV synthesis from dynamic passes," in 2017 IEEE Nuclear Science Symposium and Medical Imaging Conference (NSS/MIC), 2017: IEEE, pp. 1–6.

[88]. Viswanath V, Witherspoon MED, Karp JS, and Surti S, "Numerical observer study of lesion detectability for a long axial field-of-view whole-body PET imager using the PennPET Explorer," Phys. Med. Biol, vol. 65, no. 3, 2 2020, Art no. 035002, doi: 10.1088/1361-6560/ab6011.

[89]. Viswanath V et al., "Quantifying bias and precision of kinetic parameter estimation on the PennPET Explorer, a long axial field-of-view scanner," IEEE Transactions on Radiation and Plasma Medical Sciences pp. 1–1, 2020, doi: 10.1109/TRPMS.2020.3021315.

[90]. Wang G et al., "Total-Body Dynamic PET of Metastatic Cancer: First Patient Results," J Nucl Med, vol. 61, no. supplement 1, pp. 208–208, 2020.

[91]. Leahy R, Boellaard R, and Zaidi H, "Whole-body parametric PET imaging will replace conventional image-derived PET metrics in clinical oncology," Med Phys, no. 45, pp. 5355–5358, 2018. [PubMed: 30374995]

[92]. Foster JA and Neufeld K-AM, "Gut–brain axis: how the microbiome influences anxiety and depression," Trends in neurosciences, vol. 36, no. 5, pp. 305–312, 2013. [PubMed: 23384445]

[93]. Tahsili-Fahadan P and Geocadin RG, "Heart–brain axis: effects of neurologic injury on cardiovascular function," Circulation research, vol. 120, no. 3, pp. 559–572, 2017. [PubMed: 28154104]

[94]. Rajendran JG et al., "Hypoxia and glucose metabolism in malignant tumors: Evaluation by F-18 fluoromisonidazole and F-18 fluorodeoxyglucose positron emission tomography imaging," Clinical Cancer Research, vol. 10, no. 7, pp. 2245–2252, 4 2004, doi: 10.1158/1078-0432.ccr-0688-3. [PubMed: 15073099]

[95]. Guo JX et al., "F-18-Alfatide II and F-18-FDG Dual-Tracer Dynamic PET for Parametric, Early Prediction of Tumor Response to Therapy," J. Nucl. Med, vol. 55, no. 1, pp. 154–160, 1 2014, doi: 10.2967/jnumed.113.122069. [PubMed: 24232871]

[96]. Abraham A et al., "F-18-FDG PET Imaging of Myocardial Viability in an Experienced Center with Access to F-18-FDG and Integration with Clinical Management Teams: The Ottawa-FIVE Substudy of the PARR 2 Trial," J. Nucl. Med, vol. 51, no. 4, pp. 567–574, 4 2010, doi: 10.2967/jnumed.109.065938. [PubMed: 20237039]

[97]. Ho CL, Chen SR, Yeung DWC, and Cheng TKC, "Dual-tracer PET/CT imaging in evaluation of metastatic hepatocellular carcinoma," J. Nucl. Med, vol. 48, no. 6, pp. 902–909, 6 2007, doi: 10.2967/jnumed.106.036673. [PubMed: 17504862]

[98]. Richter JA et al., "Dual Tracer C-11-Choline and FDG-PET in the Diagnosis of Biochemical Prostate Cancer Relapse After Radical Treatment," Molecular Imaging and Biology, vol. 12, no. 2, pp. 210–217, 4 2010, doi: 10.1007/s11307-009-0243-y. [PubMed: 19543774]

[99]. Kadrmas DJ and Rust TC, "Feasibility of rapid multitracer PET tumor imaging," IEEE Trans. Nucl. Sci, vol. 52, no. 5, pp. 1341–1347, 10 2005, doi: 10.1109/tns.2005.858230.

[100]. Koeppe RA, Raffel DM, Snyder SE, Ficaro EP, Kilbourn MR, and Kuhl DE, "Dual- C-11 tracer single-acquisition positron emission tomography studies," J. Cereb. Blood Flow Metab, vol. 21, no. 12, pp. 1480–1492, 12 2001, doi: 10.1097/00004647-200112000-00013. [PubMed: 11740210]

[101]. Joshi AD, Koeppe RA, Fessler JA, and Kilbourn MR, "Signal separation and parameter estimation in noninvasive dual-tracer PET scans using reference-region approaches," J. Cereb. Blood Flow Metab, vol. 29, no. 7, pp. 1346–1357, 7 2009, doi: 10.1038/jcbfm.2009.53. [PubMed: 19401708]

[102]. Zhang JL, Morey AM, and Kadrmas DJ, "Application of separable parameter space techniques to multi-tracer PET compartment modeling," Phys. Med. Biol, vol. 61, no. 3, pp. 1238–1258, 2 2016, doi: 10.1088/0031-9155/61/3/1238. [PubMed: 26788888]

[103]. El Fakhri G, Trott CM, Sitek A, Bonab A, and Alpert NM, "Dual-Tracer PET Using Generalized Factor Analysis of Dynamic Sequences," Molecular Imaging and Biology, vol. 15, no. 6, pp. 666–674, 12 2013, doi: 10.1007/s11307-013-0631-1. [PubMed: 23636489]

[104]. Bell C et al., "Dual acquisition of F-18-FMISO and F-18-FDOPA," Phys. Med. Biol, vol. 59, no. 14, pp. 3925–3949, 7 2014, doi: 10.1088/0031-9155/59/14/3925. [PubMed: 24958083]

[105]. Bell C, Puttick S, Rose S, Smith J, Thomas P, and Dowson N, "Design and utilisation of protocols to characterise dynamic PET uptake of two tracers using basis pursuit," Phys. Med.

Biol, vol. 62, no. 12, pp. 4897–4916, 6 2017, doi: 10.1088/1361-6560/aa6b44. [PubMed: 28375137]

[106]. Xu JM and Liu HF, "Deep-Learning-Based Separation of a Mixture of Dual-Tracer Single-Acquisition PET Signals With Equal Half-Lives: A Simulation Study," IEEE Transactions on Radiation and Plasma Medical Sciences, vol. 3, no. 6, pp. 649–659, 11 2019, doi: 10.1109/trpms.2019.2897120.

[107]. Xu JM and Liu HF, "Three-dimensional convolutional neural networks for simultaneous dual-tracer PET imaging," Phys. Med. Biol, vol. 64, no. 18, 9 2019, Art no. 185016, doi: 10.1088/1361-6560/ab3103.

[108]. Andreyev A, Sitek A, and Celler A, "EM reconstruction of dual isotope PET using staggered injections and prompt gamma positron emitters," Medical Physics, vol. 41, no. 2, 2 2014, Art no. 022501, doi: 10.1118/1.4861714.

[109]. Cheng XY et al., "Direct Parametric Image Reconstruction in Reduced Parameter Space for Rapid Multi-Tracer PET Imaging," IEEE Trans. Med. Imaging, vol. 34, no. 7, pp. 1498–1512, 7 2015, doi: 10.1109/tmi.2015.2403300. [PubMed: 25700443]

[110]. Ikoma Y, Toyama H, and Suhara T, "Simultaneous quantification of two brain functions with dual tracer injection in PET dynamic study," in Quantitation in Biomedical Imaging with Pet and Mri, Iida H, Shah NJ, Hayashi T, and Watabe H Eds., (International Congress Series, no. 1265), 2004, pp. 74–78.

[111]. Kudomi N et al., "Rapid quantitative measurement of CMRO2 and GBF by dual administration of O-15-labeled oxygen and water during a single PET scan - a validation study and error analysis in anesthetized monkeys," J. Cereb. Blood Flow Metab, vol. 25, no. 9, pp. 1209–1224, 9 2005, doi: 10.1038/sj.jcbfm.9600118. [PubMed: 15874976]

[112]. Verhaeghe J and Reader AJ, "Simultaneous water activation and glucose metabolic rate imaging with PET," Phys. Med. Biol, vol. 58, no. 3, pp. 393–411, 2 2013, doi: 10.1088/0031-9155/58/3/393. [PubMed: 23296197]

[113]. Rust TC and Kadrmas DJ, "Rapid dual-tracer PTSM plus ATSM PET imaging of tumour blood flow and hypoxia: a simulation study," Phys. Med. Biol, vol. 51, no. 1, pp. 61–75, 1 2006, doi: 10.1088/0031-9155/51/1/005. [PubMed: 16357431]

[114]. Black NF, McJames S, Rust TC, and Kadrmas DJ, "Evaluation of rapid dual-tracer Cu-62-PTSM+Cu-62-ATSM PET in dogs with spontaneously occurring tumors," Phys. Med. Biol, vol. 53, no. 1, pp. 217–232, 1 2008, doi: 10.1088/0031-9155/53/1/015. [PubMed: 18182698]

[115]. Kadrmas DJ, Rust TC, and Hoffman JM, "Single-scan dual-tracer FLT+FDG PET tumor characterization," Phys. Med. Biol, vol. 58, no. 3, pp. 429–449, 2 2013, doi: 10.1088/0031-9155/58/3/429. [PubMed: 23296314]

[116]. Kadrmas DJ and Hoffman JM, "Methodology for Quantitative Rapid Multi-Tracer PET Tumor Characterizations," Theranostics, vol. 3, no. 10, pp. 757–773, 2013, doi: 10.7150/thno.5201. [PubMed: 24312149]

[117]. Rust TC, DiBella EVR, McGann CJ, Christian PE, Hoffman JM, and Kadrmas DJ, "Rapid dual-injection single-scan N-13-ammonia PET for quantification of rest and stress myocardial blood flows," Phys. Med. Biol, vol. 51, no. 20, pp. 5347–5362, 10 2006, doi: 10.1088/0031-9155/51/20/018. [PubMed: 17019043]

[118]. Alpert N, Fang YHD, and El Fakhri G, "Single-scan rest/stress imaging F-18-labeled flow tracers," Medical Physics, vol. 39, no. 11, pp. 6609–6620, 11 2012, doi: 10.1118/1.4754585. [PubMed: 23127055]

[119]. Tseng J et al., "F-18-FDG kinetics in locally advanced breast cancer: Correlation with tumor blood flow and changes in response to neoadjuvant chemotherapy," J. Nucl. Med, vol. 45, no. 11, pp. 1829–1837, 11 2004. [Online]. Available: <Go to ISI>://WOS:000225086000014. [PubMed: 15534051]

[120]. Mullani NA, Herbst RS, O'Neil RG, Gould KL, Barron BJ, and Abbruzzese JL, "Tumor blood flow measured by PET dynamic imaging of first-pass F-18-FDG uptake: A comparison with O-15-Labeled water-measured blood flow," J. Nucl. Med, vol. 49, no. 4, pp. 517–523, 4 2008, doi: 10.2967/jnumed.107.048504. [PubMed: 18344436]

[121]. Bernstine H et al., "FDG PET/CT Early Dynamic Blood Flow and Late Standardized Uptake Value Determination in Hepatocellular Carcinoma," Radiology, vol. 260, no. 2, pp. 503–510, 8 2011, doi: 10.1148/radiol.11102350. [PubMed: 21555347]

[122]. Cochet A et al., "Evaluation of Breast Tumor Blood Flow with Dynamic First-Pass F-18-FDG PET/CT: Comparison with Angiogenesis Markers and Prognostic Factors," J. Nucl. Med, vol. 53, no. 4, pp. 512–520, 4 2012, doi: 10.2967/jnumed.111.096834. [PubMed: 22343501]

[123]. Humbert O et al., "Breast Cancer Blood Flow and Metabolism on Dual-Acquisition F-18-FDG PET: Correlation with Tumor Phenotype and Neoadjuvant Chemotherapy Response," J. Nucl. Med, vol. 59, no. 7, pp. 1035–1041, 7 2018, doi: 10.2967/jnumed.117.203075. [PubMed: 29439010]

[124]. Walberer M et al., "Potential of Early F-18 −2-Fluoro-2-Deoxy-D-Glucose Positron Emission Tomography for Identifying Hypoperfusion and Predicting Fate of Tissue in a Rat Embolic Stroke Model," Stroke, vol. 43, no. 1, pp. 193–U359, 1 2012, doi: 10.1161/strokeaha.111.624551. [PubMed: 22033990]

[125]. Winterdahl M, Munk OL, Sorensen M, Mortensen FV, and Keiding S, "Hepatic Blood Perfusion Measured by 3-Minute Dynamic F-18-FDG PET in Pigs," J. Nucl. Med, vol. 52, no. 7, pp. 1119–1124, 7 2011, doi: 10.2967/jnumed.111.088278. [PubMed: 21680685]

[126]. Zuo Y, Badawi R, Foster C, Smith T, López J, and Wang G, "Multiparametric cardiac 18F-FDG PET in humans: kinetic model selection and identifiability analysis," arXiv, p. 2008.05099, 2020.

[127]. Padhani AR and Miles KA, "Multiparametric Imaging of Tumor Response to Therapy," Radiology, vol. 256, no. 2, pp. 348–364, 8 2010, doi: 10.1148/radiol.10091760. [PubMed: 20656830]

[128]. Hsiao IT et al., "Correlation of early-phase F-18-florbetapir (AV-45/Amyvid) PET images to FDG images: preliminary studies," European Journal of Nuclear Medicine and Molecular Imaging, vol. 39, no. 4, pp. 613–620, 4 2012, doi: 10.1007/s00259-011-2051-2. [PubMed: 22270508]

[129]. Asghar M, Hinz R, Herholz K, and Carter SF, "Dual-phase 18F florbetapir in frontotemporal dementia," European Journal of Nuclear Medicine and Molecular Imaging, vol. 46, no. 2, pp. 304–311, 2 2019, doi: 10.1007/s00259-018-4238-2. [PubMed: 30569187]

[130]. Ottoy J et al., "F-18-FDG PET, the early phases and the delivery rate of F-18-AV45 PET as proxies of cerebral blood flow in Alzheimer's disease: Validation against O-15-H2O PET," Alzheimers & Dementia, vol. 15, no. 9, pp. 1172–1182, 9 2019, doi: 10.1016/j.jalz.2019.05.010.

[131]. Chen YJ et al., "Relative C-11-PiB Delivery as a Proxy of Relative CBF: Quantitative Evaluation Using Single-Session O-15-Water and C-11-PiB PET," J. Nucl. Med, vol. 56, no. 8, pp. 1199–1205, 8 2015, doi: 10.2967/jnumed.114.152405. [PubMed: 26045309]

[132]. Rodriguez-Vieitez E et al., "Comparison of Early-Phase C-11-Deuterium-L-Deprenyl and C-11-Pittsburgh Compound B PET for Assessing Brain Perfusion in Alzheimer Disease," J. Nucl. Med, vol. 57, no. 7, pp. 1071–1077, 7 2016, doi: 10.2967/jnumed.115.168732. [PubMed: 26912447]

[133]. Bilgel M, Beason-Held L, An Y, Zhou Y, Wong DF, and Resnick SM, "Longitudinal evaluation of surrogates of regional cerebral blood flow computed from dynamic amyloid PET imaging," J. Cereb. Blood Flow Metab, vol. 40, no. 2, pp. 288–297, 2 2020, doi: 10.1177/0271678×19830537. [PubMed: 30755135]

[134]. Florek L et al., "Dual Time-Point F-18 Florbetaben PET Delivers Dual Biomarker Information in Mild Cognitive Impairment and Alzheimer's Disease," Journal of Alzheimers Disease, vol. 66, no. 3, pp. 1105–1116, 2018, doi: 10.3233/jad-180522.

[135]. Visser D et al., "Tau pathology and relative cerebral blood flow are independently associated with cognition in Alzheimer's disease," European Journal of Nuclear Medicine and Molecular Imaging, doi: 10.1007/s00259-020-04831-w.

[136]. Beyer L et al., "Early-phase F-18 PI-2620 tau-PET imaging as a surrogate marker of neuronal injury," European Journal of Nuclear Medicine and Molecular Imaging, doi: 10.1007/s00259-020-04788-w.

[137]. Oliveira FPM et al., "Can C-11-PiB-PET Relative Delivery R-1 or C-11-PiB-PET Perfusion Replace F-18-FDG-PET in the Assessment of Brain Neurodegeneration?," Journal of Alzheimers Disease, vol. 65, no. 1, pp. 89–97, 2018, doi: 10.3233/jad-180274.

[138]. Peretti DE et al., "Relative cerebral flow from dynamic PIB scans as an alternative for FDG scans in Alzheimer's disease PET studies," Plos One, vol. 14, no. 1, 1 2019, Art no. e0211000, doi: 10.1371/journal.pone.0211000.

[139]. Grkovski M et al., "Multiparametric Imaging of Tumor Hypoxia and Perfusion with F-18-Fluoromisonidazole Dynamic PET in Head and Neck Cancer," J. Nucl. Med, vol. 58, no. 7, pp. 1072–1080, 7 2017, doi: 10.2967/jnumed.116.188649. [PubMed: 28183993]

[140]. Richard MA, Fouquet JP, Lebel R, and Lepage M, "Determination of an Optimal Pharmacokinetic Model of F-18-FET for Quantitative Applications in Rat Brain Tumors," J. Nucl. Med, vol. 58, no. 8, pp. 1278–1284, 8 2017, doi: 10.2967/jnumed.116.180612. [PubMed: 28765227]

[141]. Wang GB, "High temporal-resolution dynamic PET image reconstruction using a new spatiotemporal kernel method," IEEE Trans. Med. Imaging, vol. 38, no. 3, pp. 664–674, 2019. [PubMed: 30222553]

[142]. Hong I, Cho SH, Michel CJ, Casey ME, and Schaefferkoetter JD, "Complementary frame reconstruction: a low-biased dynamic PET technique for low count density data in projection space," Phys. Med. Biol, vol. 59, no. 18, pp. 5441–5455, 9 2014, doi: 10.1088/0031-9155/59/18/5441. [PubMed: 25164868]

[143]. Kuhnel C, Seifert P, Drescher R, and Freesmeyer M, "Reconstruction method to combine high temporal resolution with appropriate image quality in dynamic PET angiography," European Journal of Nuclear Medicine and Molecular Imaging, vol. in press, 2020, doi: 10.1007/s00259-020-04962-0.

[144]. Wang G and Qi J, "PET image reconstruction using kernel method," IEEE Trans. Med. Imaging, vol. 34, no. 1, pp. 61–71, 2015. [PubMed: 25095249]

[145]. Zhang X, Cherry SR, Xie Z, Shi H, Badawi RD, and Qi J, "Subsecond total-body imaging using ultrasensitive positron emission tomography," Proc Natl Acad Sci U S A, vol. 117, no. 5, pp. 2265–2267, 2 4 2020, doi: 10.1073/pnas.1917379117. [PubMed: 31964808]

[146]. Wang GB, Sarkar S, Kim E, and Badawi RD, "Time-varying kinetic modeling of high temporal-resolution dynamic 18F-FDG PET data for multiparametric imaging," J. Nucl. Med, vol. 59, no. supplement 1, pp. 503–503, 2018.

[147]. Wang G et al., "Quantification of Glucose Transport Using High Temporal Resolution Dynamic PET Imaging," J. Nucl. Med, vol. 60, no. supplement 1, pp. 521–521, 6 22–25 2019.

[148]. Zuo Y, Cherry S, Badawi R, and Wang G, "Multiphase Patlak Plot Enabled by High Temporal Resolution Total-body Dynamic PET," J Nucl Med, vol. 61, no. supplement 1, pp. 207–207, 2020.

[149]. Gong K, Berg E, Cherry SR, and Qi JY, "Machine Learning in PET: From Photon Detection to Quantitative Image Reconstruction," Proceedings of the IEEE, vol. 108, no. 1, pp. 51–68, 1 2020, doi: 10.1109/jproc.2019.2936809.

[150]. Reader A, Corda G, Mehranian A, da Costa-Luis C, Ellis S, and Schnabel J, "Deep Learning for PET Image Reconstruction," IEEE Transactions on Radiation and Plasma Medical Sciences 2020, doi: 10.1109/TRPMS.2020.3014786.

(a)

(b)
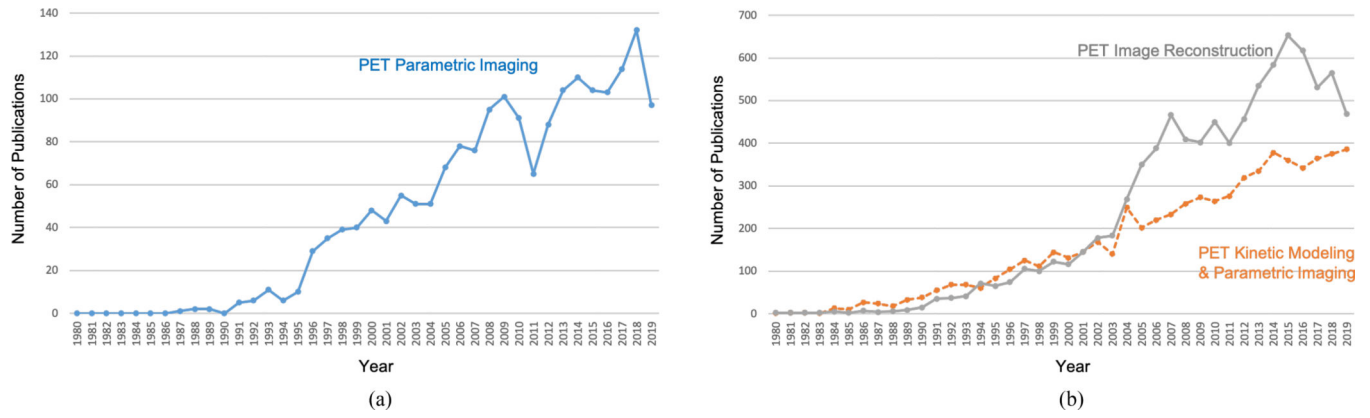
Fig. 1.
Historic trends of productivity as recorded in PubMed for the period from 1980–2019.
Shown are yearly number of publications on (a) 'PET parametric imaging', and (b) ['PET
Kinetic' OR 'PET Parametric Imaging'] (orange) and 'PET image reconstruction' (gray).
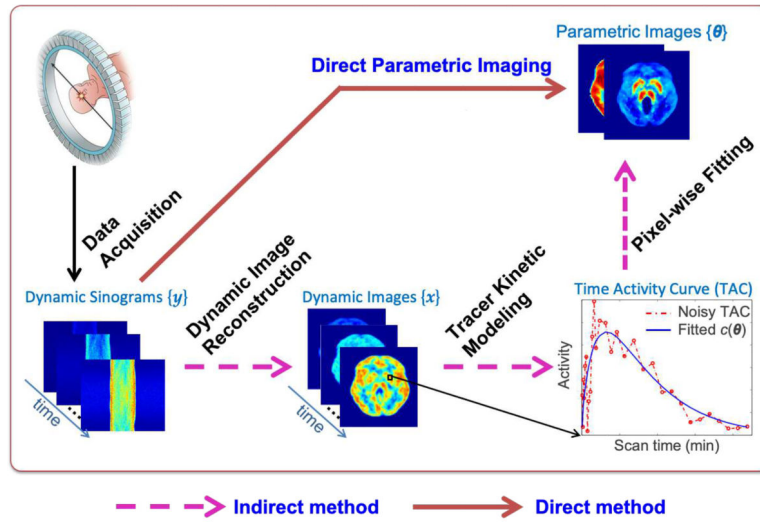
Fig. 2.
Graphical illustration of parametric imaging of tracer kinetics. The indirect method consists of dynamic image reconstruction followed by tracer kinetic modeling. The direct method estimates the parametric images directly from the raw projection data.
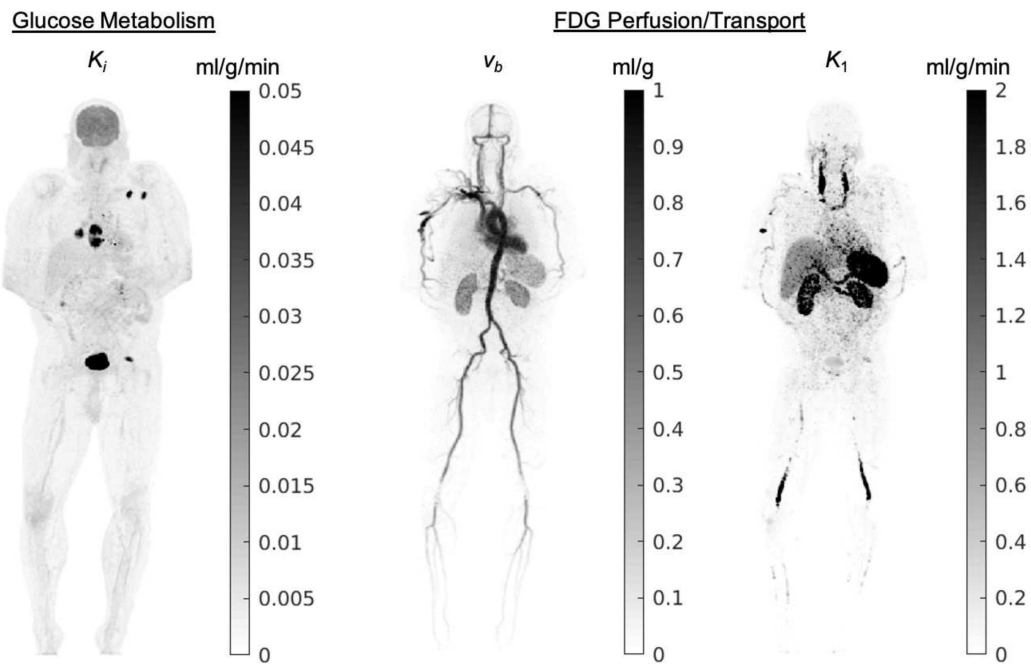
Fig. 3.
Total-body PET multi-parametric images of FDG metabolism (net influx rate K_i) and FDG perfusion/transport parameters (blood-to-tissue transport rate K_1 and fractional blood volume v_b).
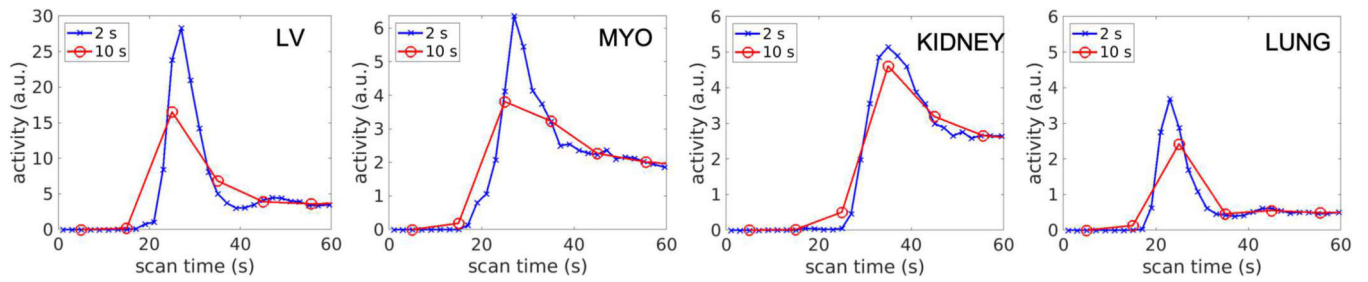
Fig. 4:
Comparison of high-temporal resolution (2s/frame) and standard temporal resolution (10s/frame) for regional time activity curves (TACs) in different regions of interest (ROIs): left ventricle (LV), myocardium, kidney (renal cortex) and lung. Shown are the first one-minute data extracted from a dynamic ^{18}F-FDG PET scan performed on the EXPLORER scanner.

Author Manuscript

Author Manuscript

Author Manuscript

Author Manuscript

TABLE I

LIST OF REVIEW ARTICLES ON KINETIC MODELING

Year	Authors	Focus
2001	Gunn, Gunn, Cunningham [29]	General compartmental modeling theory
2001	Ichise, Meyer, Yonekura [30]	Neuroreceptor quantification models
2011	Zanotti-Fregonara et al. [47]	Image-derived input functions for brain PET
2014	Kotasidis, Tsoumpas, Rahmim [10]	Kinetic modeling towards clinical adoption, including blood input function estimation and PET/MR kinetic modeling
2018	Murthy et al. [3]	A position paper on clinical quantification of myocardial blood flow using PET.
2020	Feng, Wen, Chen [48]	Noninvasive estimation of blood input functions

TABLE II

LIST OF REVIEW ARTICLES ON DYNAMIC PET RECONSTRUCTION

Year	Authors	Focus
2008	Tsoumpas, Turkheimer, Thielemans [50]	Indirect and direct approaches for linear parametric imaging
2009	Rahmim, Tang, Zaidi [51]	Indirect and direct approaches for dynamic PET parametric imaging
2013	Wang & Qi [52]	Overview of optimization algorithms for direct parametric reconstruction
2014	Reader & Verhaeghe [11]	4D image reconstruction approaches
2019	Gallezot et al. [9]	Overview of methods for addressing the challenges of noise suppression, input functions, and motion correction in parametric imaging
2019	Rahmim et al. [15]	Overview of the principle, potentials, and applications of dynamic whole-body parametric imaging

TABLE III

List of different software for kinetic modeling and parametric imaging. Top part contains software in different applications (e.g. brain; oncology), while bottom lists cardiac-dedicated software.

Software	Vendor/Developer	Commercial vs. Free	Parametric Imaging	URL
APPIAN	Thomas Funck	Free	✓	github.com/APPIAN-PET/APPIAN
COMKAT	Case Western Reserve University	Free		comkat.case.edu
DEPICT	Roger Gunn	Free	✓	bic.mcgill.ca/~rgunn/DEPICT
Imager4D	Johns Hopkins University	Free	✓	jeffreyleal.wixsite.come/jleal
Imlook4d	Jan Axelsson	Free	✓	sites.google.com/site/imlook4d
Kinfitr	Granville Matheson	Free		github.come/mathesong/kinfitr
KIS	UCLA	Free		kis.nuc.ucla.edu
Magia	Turku PET Centre	Free	✓	github.com/tkarjal/magia
mFEVolve	MultiFunctional Imaging	Commercial	✓	MFImage.com
MIAKAT	Graham Searle & Roger Gunn	Free	✓	miakat.org
MITK Model Fit	German Cancer Research Center	Free	✓	mitk.org/wiki/MITK-ModelFit
Multiparametric PET Suite AI	Siemens	Commercial	✓	siemens-healthineers.com
PKIN	PMOD	Commercial		pmod.com
PXMOD	PMOD	Commercial	✓	pmod.com
Qmodeling	FGUMA	Free	✓	uimcimes.es
SAAM II	The Epsilon Group	Commercial		tegvirginia.com
SAKE	University of Padua	Free	✓	bio.dei.unipd.it/sake/cgi-bin/index.cgi
SPAMALIZE	Terry Oakes & Waisman Lab for Functional Brain Imaging	Free	✓	brainimaging.waisman.wisc.edu/~oakes
TKMF	UCLA	Free		dragon.nuc.ucla.edu/modelfitting
VINCI	Max Planck Institute for Metabolism Research	Free	✓	vinci.sf.mpg.de
VivoQuant	Invicro	Commercial	✓	vivoquant.com
4DM	INVIA	Commercial (Cardiac)	✓	inviasolutions.com
Carimas	Turku PET Centre	Commercial (Cardiac)	✓	turkupetcentre.fi/carimas
FlowQuant	University of Ottawa Heart Institute	Commercial (Cardiac)	✓	ottawaheart.ca
HeartSee	Bracco Diagnostics	Commercial (Cardiac)	✓	cardiogen.com/heartsee
ImagenQ	CVIT	Commercial (Cardiac)	✓	cvit.com/products/imagenq
MunichHeart	Technical University of Munich	Free (Cardiac)	✓	munichheart.de

Software	Vendor/Developer	Commercial vs. Free	Parametric Imaging	URL
PCARD PET	PMOD	Commercial (Cardiac)	✓	pmod.com
QPET	Cedars-Sinai	Commercial (Cardiac)	✓	cedars-sinai.org
Syngo MBF	Siemens	Commercial (Cardiac)	✓	siemens-healtinheers.com

TABLE IV

Examples of Clinical PET Scanners with Wide AFOV as Compared to a typical conventional PET scanner GE Discovery 690

PET Scanner	GE Discovery 690 [67]	GE Discovery MI (5-ring) [65]	Siemens Biograph Vision [64]	Canon Cartesion Prime [66]	UIH uEXPLORER [18]
Year coming into the market	2010	2018	2018	2019	2019
Axial field of view (cm)	**16**	**25**	**26**	**27**	**194**
Spatial resolution (mm)	4.7	4.3	3.6	5.0	2.9
NEMA sensitivity (cps/kBq)	7.5	20.8	16.4	13.0	171
Time-of-flight resolution (ps)	544	382	210	260	505
Effective gain in sensitivity	**1.0**	**4.0**	**5.7**	**3.6**	**24.6**